Wave-front error measurements and alignment of CLASP2 telescope with a dual-band pass cold mirror coated primary mirror

Masaki Yoshida[a,b], Donguk Song[b], Ryohko Ishikawa[b], Ryouhei Kano[b], Yukio Katsukawa[b], Yoshinori Suematsu[b], Noriyuki Narukage[b], Masahito Kubo[b], Kazuya Shinoda[b], Takenori J. Okamoto[b], David E. McKenzie[c], Laurel A. Rachmeler[c], Frédéric Auchère[d], and Javier Trujillo Bueno[e]

[a]Department of Astronomical Science, School of Physical Sciences, SOKENDAI (The Graduate University for Advanced Studies), 2-21-1 Osawa, Mitaka, Tokyo 181-8588, Japan
[b]National Astronomical Observatory of Japan, 2-21-1 Osawa, Mitaka, Tokyo, 181-8588, Japan
[c]NASA Marshall Space Flight Ctr., Huntsville, AL, 35812, USA
[d]Institut d'Astrophysique Spatiale, CNRS/Univ. Paris-Sud 11, B, UTF02C6atiment 121, 91405 Orsay, France
[e]Instituto de Astrofísica de Canarias, 38205 La Laguna, Tenerife, Spain

ABSTRACT

"Chromospheric LAyer Spectro-Polarimeter (CLASP2)" is the next sounding rocket experiment of the "Chromospheric Lyman-Alpha Spectro-Polarimeter (CLASP)" that succeeded in observing for the first time the linear polarization spectra in the hydrogen Lyman-α line (121.6 nm) and is scheduled to be launched in 2019. In CLASP2, we will carry out full Stokes-vector spectropolarimetric observations in the Mg II h & k lines near 280 nm with the spectro-polarimeter (SP), while imaging observations in the Lyman-α line will be conducted with the slitjaw optics (SJ). For the wavelength selection of CLASP2, the primary mirror of the telescope uses a new dual-band pass cold mirror coating targeting both at 121.6 nm and 280 nm. Therefore, we have to perform again the alignment of the telescope after the installation of the recoated primary mirror. Before unmounting the primary mirror from the telescope structure, we measured the wave-front error (WFE) of the telescope. The measured WFE map was consistent with what we had before the CLASP flight, clearly indicating that the telescope alignment has been maintained even after the flight. After the re-coated primary mirror was installed the WFE was measured, and coma aberration was found to be larger. Finally, the secondary mirror shim adjustments were carried out based on the WFE measurements. In CLASP2 telescope, we improved a fitting method of WFE map (applying 8th terms circular Zernike polynomial fitting instead of 37th terms circular Zernike fitting) and the improved method enables to achieve better performance than CLASP telescope. Indeed, WFE map obtained after the final shim adjustment indicated that the required specification (< 5.5 μm RMS spot radius) that is more stringent than CLASP telescope was met.

Keywords: Sun, Optical alignment, CLASP2 project, UV spectropolarimetry, Sounding rocket experiment

1. INTRODUCTION

The "Chromospheric Lyman-Alpha Spectro-Polarimeter (CLASP)"[1–3] was launched in 2015 by a NASA sounding rocket, and succeeded in the first observation of the linear polarization spectra of the hydrogen Lyman-α line (121.6 nm).[4] The CLASP sounding rocket experiment was conducted with the purpose of opening up a diagnostic window for exploring the chromospheric magnetic field of the Sun using the Hanle effect. The Hanle effect is the magnetic-field-induced modification of the linear polarization produced by scattering processes in a spectral line. Therefore, for deriving the magnetic field using the Hanle effect in a single spectral line, it is necessary to

Further author information: (Send correspondence to Masaki Yoshida)
Masaki Yoshida: E-mail: masaki.yoshida@nao.ac.jp, Telephone: +81-422-34-3715

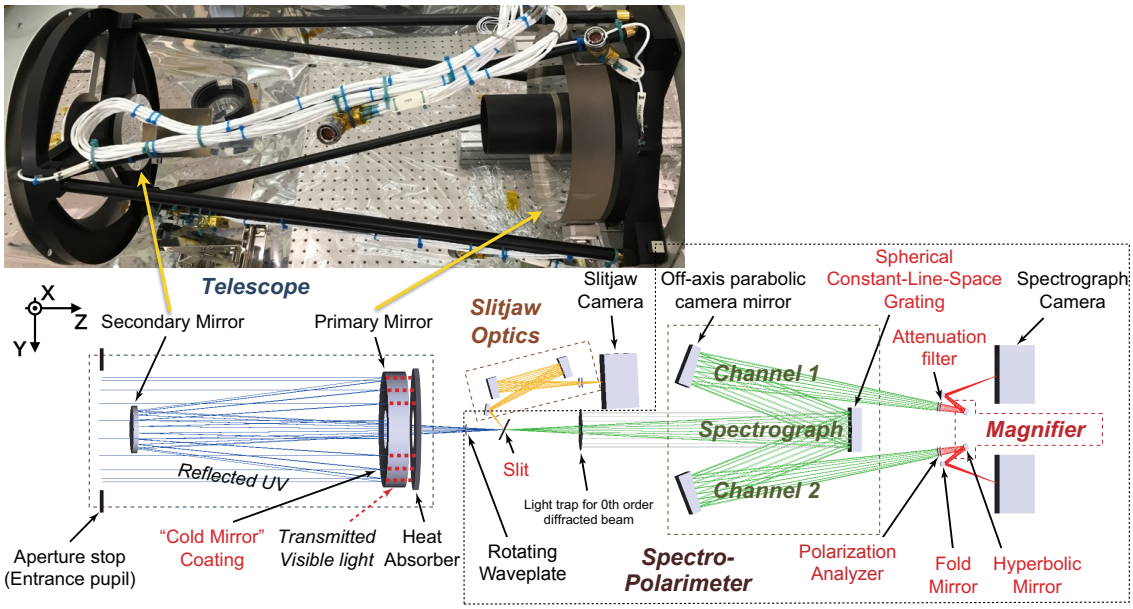

Figure 1. CLASP2 telescope (top) and CLASP2 Instrument design (bottom).[9] Coordinate of CLASP2 instrument is described in the left. The Z-axis positive is in direction from the telescope to the spectro-polarimeter (SP), the Y-axis positive direction is opposite side to slitjaw optics (SJ), and the X-axis is defined by left-handed system.

predict the polarized light originating in the absence of the magnetic field. Fortunately, there are other spectral lines whose core originates also in the upper solar chromosphere and whose sensitivity to the Hanle effect is complementary to that of Lyman-α.[5] In particular, the Mg II k line at 279.6 nm is sensitive to weaker magnetic field than Lyman-α. In addition to the Hanle effect, the circular polarization induced by the Zeeman effect can be measurable in Mg II h (280.4 nm) & k lines by sampling strong-field regions.[6–8] Therefore, "Chromospheric LAyer Spectro-Polarimeter (CLASP2)"[9] is being promoted as a re-flight plan of CLASP for measuring the four Stokes profiles across the Mg II h & k lines. The CLASP payload was recovered, and in 2019 we plan to launch it again after refitting the existing CLASP instrument (Figure 1). The slitjaw optics (SJ) remains unchanged from the first flight and the images in the Lyman-α passband will be taken.[10,11] For these wavelength selections, a new dual-band pass cold mirror coating targeting both at 121.6 nm and 280 nm is applied to the primary mirror of the telescope. Therefore, we have to perform again the alignment of the telescope after the installation of the recoated primary mirror. Our goal is to achieve the RMS spot radius of < 5.5 μm in telescope on-axis and off-axis (field-of-view (FOV): $\pm 100''$) optical pass by the optical alignment. The alignment result of spectro-polarimeter (SP) part is reported separately in Song et al.[12]

1.1 Specifications and Requirement

The specifications of CLASP2 telescope are shown in Table 1. They have not changed except for the primary mirror coating. The secondary mirror is designed to be relatively large with respect to the primary mirror because of the following two reasons. First, we try to have a smaller magnification in the secondary mirror to relax the alignment tolerance. Secondly, in order to avoid the stray light, the secondary mirror must be large enough to be illuminated by the beam from the full disk of the sun.

Requirement of CLASP2 telescope is summarized in Table 2. The science requirement for the spatial resolution combining the telescope and spectro-polarimeter (SP) is $2''$ in the $\pm 100''$ FOV (i.e. at the edge of SP FOV). Therefore, RMS spot radius must be less than $1''$ that corresponds to 24.6 μm as the spatial plate scale is $0.529''$ at the spectrograph camera with a pixel size of 13 μm. The RMS spot radius of 13 μm is allocated to SP part.[12] Taking into account the spatial magnification of the SP of 1.947, the tolerance of the RMS spot radius for the telescope is calculated to be $\sqrt{(24.6)^2 - (13)^2}/1.947 = 10.7$ μm at the slit (i.e. telescope focus) position. From this value, the spatial resolution only in the telescope part is calculated to be $1.7''$ (twice the RMS spot

Table 1. Telescope specifications.[9]

Type	Cassegrain
Aperture	ϕ270 mm
Effective Focal Length	ϕ2614.0 mm (F/9.68)
Primary Mirror	ϕ300 mm, Conic constant: -1 (Paraboloid), Curvature radius: 2054.5 mm
Secondary Mirror	ϕ123 mm, Conic constant: -5.27 (Hyperboloid), Curvature radius: 1243.0 mm
Visible Light Rejection	"Cold Mirror" coating (targeting at 121 nm and 280 nm) on primary mirror
Plate scale	$1.03''/13$ μm

radius times the plate scale of the telescope of $1.03''/13$ μm). The telescope focus alignment will be separately performed when we combine the telescope with the SP. By allocating the RMS spot radius of 9.2 μm for the defocus as in the CLASP telescope,[13] the RMS spot radius is required to be less than $\sqrt{(10.7)^2 - (9.2)^2} = 5.5$ μm with the WFE measurement.

Table 2. RMS spot radius requirement for CLASP2 telescope and corresponding spatial resolution (i.e. twice the RMS spot radius times the plate scale.)

	Spatial RMS spot radius	Spatial Resolution
Defocus	9.2 μm	-
Aberration	5.5 μm	$0.87''$
Telescope Total	10.7 μm	$1.7''$

2. MEASUREMENT AND ANALYSIS

2.1 Measurement Method

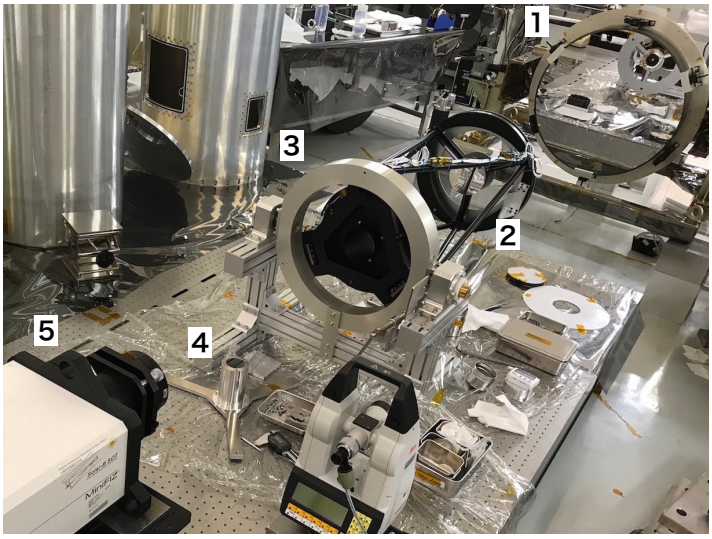

Figure 2. Double-pass configuration for the telescope alignment. 1: Plane mirror, 2: Entrance aperture and secondary mirror, 3: Primary mirror, 4: Mirror target, 5: Laser interferometer on a 6-axis stage.

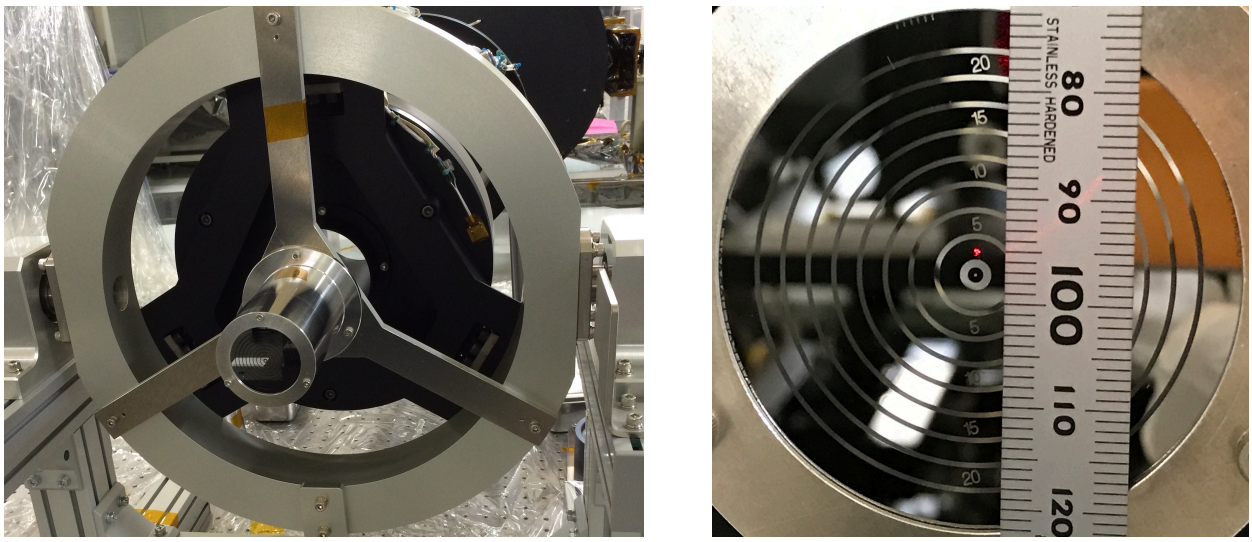

Figure 3. Left: Mirror target installed at the back side of a primary mirror using a spider and cylinder. Right: Enlargement of a mirror target.

Reflection on the mirrors does not depend on the wavelength and we carry out the telescope alignment in the visible light instead of UV. Using a He-Ne interferometer (632.8 nm), WFE of the telescope was measured, and then alignment by shimming the secondary mirror was performed. Although the primary mirror is coated with the "cold-mirror" coating, the He-Ne laser is bright enough to perform interference measurements. The procedure is the same as in CLASP telescope.[13–15] Figure 2 shows the experimental configuration, consisting of the telescope (primary mirror, secondary mirror and supporting mechanism), He-Ne laser interferometer, and plane mirror ($\phi = 600$ mm, 15 nm RMS WFE). The beam emitted from the interferometer goes through the telescope, is then reflected by the plane mirror set in front of the telescope, goes through the telescope part again, and returns to the laser interferometer (double-pass configuration). The laser interferometer measures interference fringes between the outgoing and incoming beams. First, we align the interferometer with the telescope using a mirror target. As shown in the right panel of Figure 3, reflecting and non-reflecting surfaces are concentrically formed on the mirror target. The mirror target is installed at the back side of the primary mirror using a spider consisting of three legs and a cylinder jig (left panel of Figure 3) to represent the slit location. The surface normal of the mirror target represents the optical axis of the telescope (Z-axis). The interferometer was adjusted using a 6-axis stage to make a null fringe (i.e. single large interference fringe covering the entire detector). Once we have made a null fringe, the alignment of the interferometer and the telescope was completed. Note that alignment was performed at the center position of the mirror target in the measurement of the telescope on-axis optical pass (Section 5.2), but at the locations ± 2.5 mm (X- or Y-axis) away from the center in the measurement of the telescope off-axis optical pass (Section 5.3). Next, we align the plane mirror with the telescope by getting a null fringe again.

The interferometer measurement is based on the phase-carrier method,[16] and in order to cancel the aberration caused by the measurement, the WFE was obtained with positive-tilt and negative-tilt on the reference plane. The final WFE was obtained from the average of both. The measurement was made in the atmosphere. To suppress the influence of air turbulence and increase the signal-to-noise ratio, 20 images were acquired for each of positive-tilt and negative-tilt on the reference plane and averaged. To derive the WFE, the program developed in the CLASP (first flight) telescope alignment[13–15] was used. More specifically, the interference fringe obtained by a laser interferometer is Fourier transformed to derive the power spectrum of interference fringes. After removing the pattern of the telescope's spider and the secondary mirror obscuration from these power spectra, inverse Fourier transformation was conducted to obtain the WFE map. Finally, optical aberrations were evaluated by fitting the WFE map.

2.2 Analysis Method

2.2.1 Aberration and Strategy for Alignment

Optical aberration was obtained by fitting the WFE map with Zernike polynomials. Zernike polynomials include low order terms like piston, tilt X/Y, defocus, astigmatism 0°/45°, coma X/Y, and high order terms. In the CLASP2 telescope optical alignment, we focus on low order terms. The low order terms of piston and tilt X/Y are mainly caused by air fluctuation and vibration of the ground, and do not affect the image distortion. Therefore we do not perform any adjustment for them. Defocus is caused by the despace (along Z-axis) of each of the primary mirror and secondary mirror. This effect can be adjusted by inserting shims at the base of the secondary mirror. However, the final focus adjustment with the stroke of ± 0.5 mm corresponding to $\pm 0.50\lambda$[13,15] will be performed when the telescope is combined to the SP. Thus, the defocus was not discussed using the WFE measurement if absolute value is smaller than 0.50λ. Coma aberrations are caused by decenter (shift in X- and Y-axes) and tilt of the primary and secondary mirrors. The coma aberrations can be removed by adjusting the tilt of the secondary mirror with shims. Astigmatism 0°/45° are caused by deformation of the mirror due to gravity and deformation of the mirror itself. The influence of gravity is removed by rotating the telescope by 120°, measuring WFE with these three configurations (called as 0°, 120°, 240° configurations), and averaging all measurements (Zero-G map). The influence of the inherent deformation of the mirror appears in high order terms as well as in astigmatism. These aberrations are hard to remove in the alignment but are estimated to be small from the individual surface figure measurements of the primary and secondary mirrors. In summary, in the telescope alignment, we focus on defocus and coma X/Y. Note that multiple iteration between measurements and shim adjustment were carried out to reach the final performance (Section 5.1).

2.2.2 Fitting Method

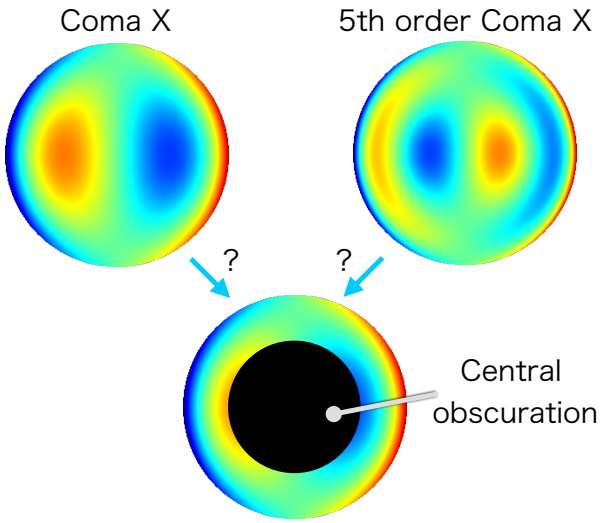

Figure 4. Example of independency caused by central obscuration (Coma X can be interpreted by 5th order Coma X due to the central obscuration.)

When the WFE was measured in the CLASP telescope alignment, fitting was performed using the 37th terms circular Zernike polynomials. However, it was found, in the course of the CLASP2 telescope alignment, that this fitting method has the following problem: As discussed in Section 1.1, our telescope has a large central obscuration by the secondary mirror. As a result, the orthogonality in the circular Zernike polynomials does not hold. More precisely, higher order terms and lower order terms in defocus and coma aberrations are not independent from each other (see example in Figure 4). Because of this, defocus and coma aberrations were not uniquely determined, and large uncertainties arose in these terms. Therefore, in the CLASP2 telescope analysis, we decide to carry out the fitting with only 8th low order terms.

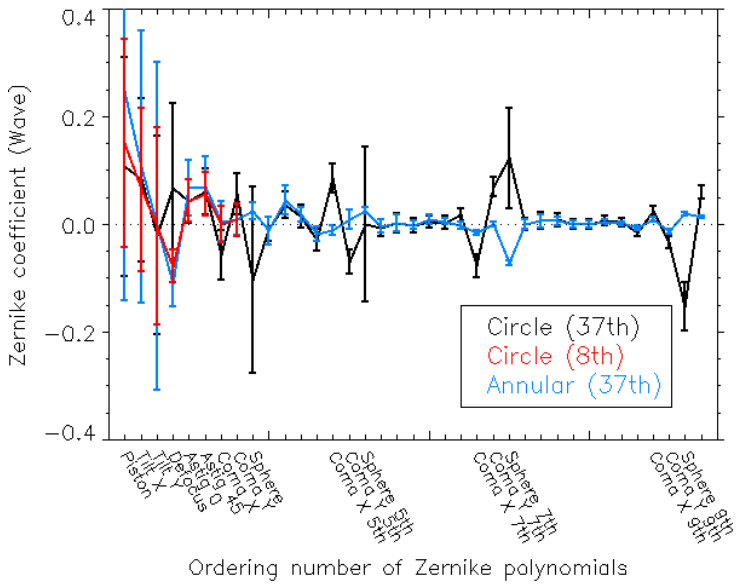

Figure 5. Zernike polynomials fitting results in each method; 8th terms circular Zernike fitting (red line), 37th terms circular Zernike fitting (black line) and 37th terms annular Zernike fitting (sky-blue line). The final measurement data at 0° configuration was calculated. Each error bars came from standard deviation of 40 images.

Figure 5 shows the comparison of fitting methods (8th terms circular Zernike polynomials in red and 37th terms circular polynomials in black). The measurement data was taken at the 0° configuration (gravity is in negative X direction) after the final shim adjustment. The error bars are the standard deviations of the 40 images (20 data of positive-tilt and negative-tilt). The value and error bar size of piston, tilt X/Y, astigmatism 0°/45° are similar between the case of 8th terms and the case of 37th terms circular fitting. However, the error bars of defocus and coma X/Y in the 8th terms circular fitting are smaller than in the 37th fitting. For example, the errors of coma aberration in the 37th terms circular fitting and the 8th terms circular fitting are $\sim 0.03\lambda$ and $< 0.02\lambda$, respectively. In addition, in 37th terms circular Zernike fitting, spherical aberrations (high order terms of defocus) and high order coma X/Y have large values and large error bars. In particular, in the CLASP telescope alignment in 2014, the standard deviation of defocus in the 37th terms circular Zernike fitting was as large as 0.10λ, and it was concluded that the cause of this was air turbulence.[13,15] By carrying out the 8th terms circular fitting this time, we confirmed that the standard deviation of defocus is reduced to less than 0.02λ and that fitting method was the cause of the large standard deviation in the CLASP telescope alignment.

Another way to solve the issue of 37th terms circular Zernike polynomials fitting is to apply 37th terms annular Zernike polynomials. As show in Figure 5 (see sky-blue line), we found that both values and error bars in higher order coefficients are reduced in 37th terms annular Zernike polynomials and that the low order terms were almost the same as those in the 8th terms circular fitting. These results clearly indicate that fitting using only 8th low order circular terms is sufficient for our alignment handling only low order terms. All the results of the subsequent analysis are obtained by 8th terms circular fitting.

3. TELESCOPE ALIGNMENT CHECK AFTER THE FIRST FLIGHT

After the first flight in 2015, the recovered instrument was shipped to Japan, and the telescope WFE was measured again in 2017. Figure 6 shows the WFE maps measured before and after the CLASP flight. In these WFE maps, piston, tilt X/Y, defocus and gravity effect were removed. Then the 8th terms circular Zernike fitting was applied, and aberration coefficients were obtained (Table 3). The difference in aberration coefficients between before and after the CLASP flight are smaller than the measurement error, clearly indicating that the alignment of the telescope is maintained between before and after the CLASP flight. Then, we proceeded to removing the primary mirror for re-coating.

Moreover, Table 3 shows that further alignment is possible as the aberration coefficients of coma Y are larger than the error in both cases. In the case of the CLASP WFE measurement, measurement error was about 0.03λ because 37th terms circular Zernike fitting was performed and we were not able to achieve the better performance than those in Table 3. However, the measurement error in the 8th terms circular Zernike fitting is now reduced to less than 0.02λ, indicating that we can achieve better performance than the CLASP telescope.

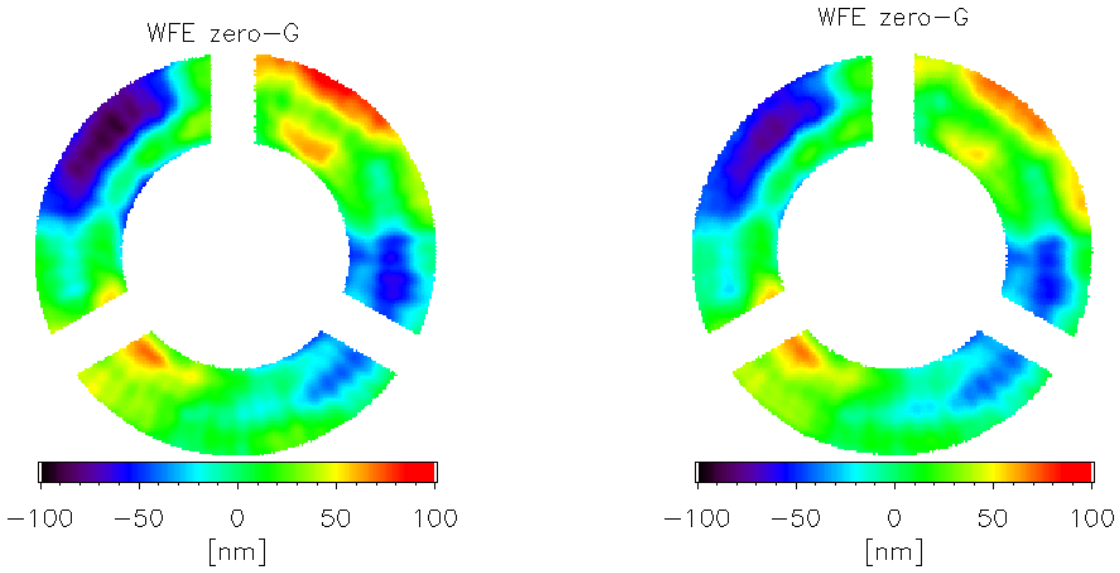

Figure 6. Zero-G WFE map before (left) and after (right) the CLASP flight. Piston, tilt X/Y, defocus and gravity effect were removed.

Table 3. Aberration coefficients derived from the 8th term circular Zernike polynomial fitting before and after the CLASP flight.

Configuration	Defocus	Astigma--tism 0°	Astigma--tism 45°	Coma Y	Coma X	RMS WFE
Before CLASP flight	0.093λ	-0.034λ	0.091λ	0.041λ	-0.010λ	37.39 nm
Error (1σ)	±0.009λ	±0.016λ	±0.015λ	±0.011λ	±0.009λ	-
After CLASP flight	−0.409λ	-0.021λ	0.081λ	0.047λ	-0.006λ	32.80 nm
Error (1σ)	±0.010λ	±0.015λ	±0.016λ	±0.012λ	±0.013λ	-

4. NEW CLASP2 COATING FOR PRIMARY MIRROR: DUAL-BAND PASS COLD MIRROR COATING

According to the change of observing wavelength windows from CLASP (121.6 nm for SP and SJ) to CLASP2 (121.6 nm for SJ and 280 nm for SP), we developed a "dual-band pass" cold mirror coating targeting at 121.6 nm and 280 nm and applied it to the primary mirror (Figure 7). The "cold mirror" coating is a narrowband multilayer coating that reflects the targeting wavelength but is transparent to the visible light and plays an important role to decrease the visible light contamination to the subsequent optical components as demonstrated in CLASP.[17] The reflectivities of the witness samples that were simultaneously coated with the primary mirror were measured as shown in Figure 8. The measured performance meets our requirement for the reflectivity around 121.6 $\pm$ 0.5 nm and 280.0 $\pm$ 1.0 nm (higher than 40% and 70%, respectively) and the non-uniformity of

reflectivity (difference between maximum and minimum reflectivities are less than 5%) at 280 nm. The uniformity is important to suppress the spurious (instrumental) polarization.[18] In addition, the reflectivity in the visible light was measured to 5% on average (right panel of Figure 8), leading to the significant reduction of the visible light.

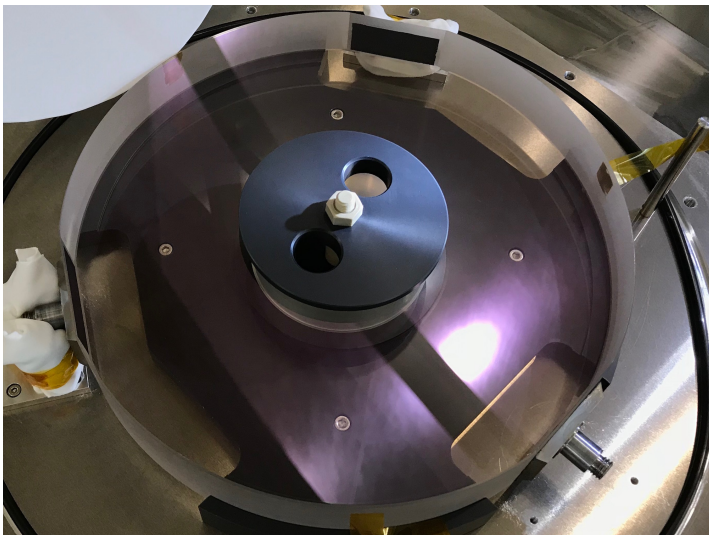

Figure 7. Primary mirror with the dual-band pass cold mirror coating.

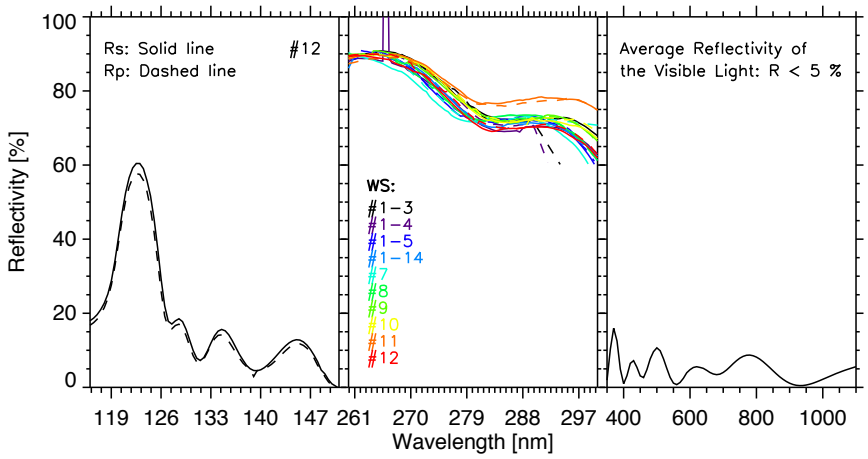

Figure 8. Measured reflectivity of dual-band pass cold mirror coating on the primary mirror. The target wavelengths are Lyman-α at 121.6 nm (left) for slitjaw optics and Mg II h & k at 280 nm (middle) for spectro-polarimeter. The primary mirror is too large to be measured and 10 witness samples that were simultaneously coated with the primary mirror were measured to confirm the performance. Only #11 (orange line) was coated on the different coating table from other witness samples, and it can be ignored from the viewpoint of coating uniformity. In UV range (left and middle), the solid and dashed lines represent the reflectivities for s- and p-polarizations measured at AOI (angle of incident) of 4° by ourselves at the synchrotron facility. In visible light range (right), reflectivity was measured at the AOI of 15° by a coating vender.

Table 4. History of shim thickness at positions of A, B and C (see right panel of Figure 9), and aberration coefficients of coma X/Y from Zero-G WFE.

Measurement note	A [μm]	B [μm]	C [μm]	Coma Y	Coma X
Before CLASP flight	0	40	100	0.041λ	-0.010λ
After CLASP flight Before primary mirror recoating	0	40	100	0.047λ	-0.006λ
After primary mirror recoating #1	0	40	100	0.061λ	-0.077λ
After primary mirror recoating #2	0	20	80	0.088λ	-0.048λ
After primary mirror recoating #3	0	60	80	0.030λ	-0.032λ
After primary mirror recoating #4	0	80	60	0.000λ	0.003λ

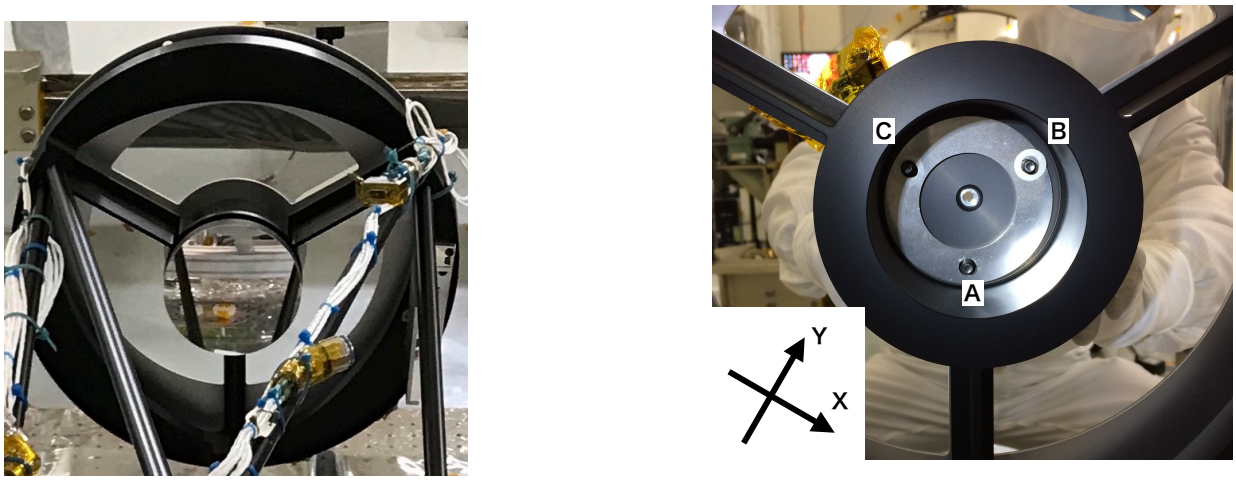

Figure 9. Left: Secondary mirror and its holder. Right: Secondary mirror's holder (seen when the secondary mirror was removed). This photo was taken at 240° configuration. Coordinate of CLASP2 instrument is described in the bottom left. Screws to fix the secondary mirror are seen. We inserted annular shims to each screws.

5. TELESCOPE ALIGNMENT AFTER RE-COATING

5.1 History of Shim Adjustment of Secondary Mirror

Table 4 shows the thickness and positions of inserted shims at the base of the secondary mirror (Figure 9) and aberration coefficients of coma X and Y for each measurement. The difference between before the CLASP flight ("Before CLASP flight" in Table 4) and after the CLASP flight ("After CLASP flight" in Table 4) was smaller than the measurement error ($1\sigma < 0.02\lambda$) as discussed in Section 3. On the other hand, it was found that the coma aberration had changed and become larger in the measurement after removing and reinstalling the primary mirror for the re-coating ("After primary mirror recoating #1–3" in Table 4). This was because a misalignment occurred when re-coated primary mirror was installed. Thus, we had adjusted the tilt of the secondary mirror using shims. By changing the thickness of shims at the positions of "B" and "C" in the right panel of Figure 9, finally we succeeded in reducing coma aberration to a small value ("After primary mirror recoating #4" in Table 4). In all measurements, the absolute values of defocus were found to be less than 0.10λ (e.g. Table 5), and such values can be adjusted when we combine the telescope with SP. Therefore, in the telescope alignment based on the WFE, shim adjustment was not done for defocus.

5.2 On-axis measurement

Final measurement results of the WFE in the three configurations (0°, 120° and 240°) are shown in Figure 10. Black arrows indicate the direction of the gravity, and it rotates so that the orientation of the three configurations

match. Each configuration's WFE maps are different because the direction of the gravity is different. In Table 5, the aberration coefficients extracted from the 8th terms circular Zernike polynomials fitting are tabulated.

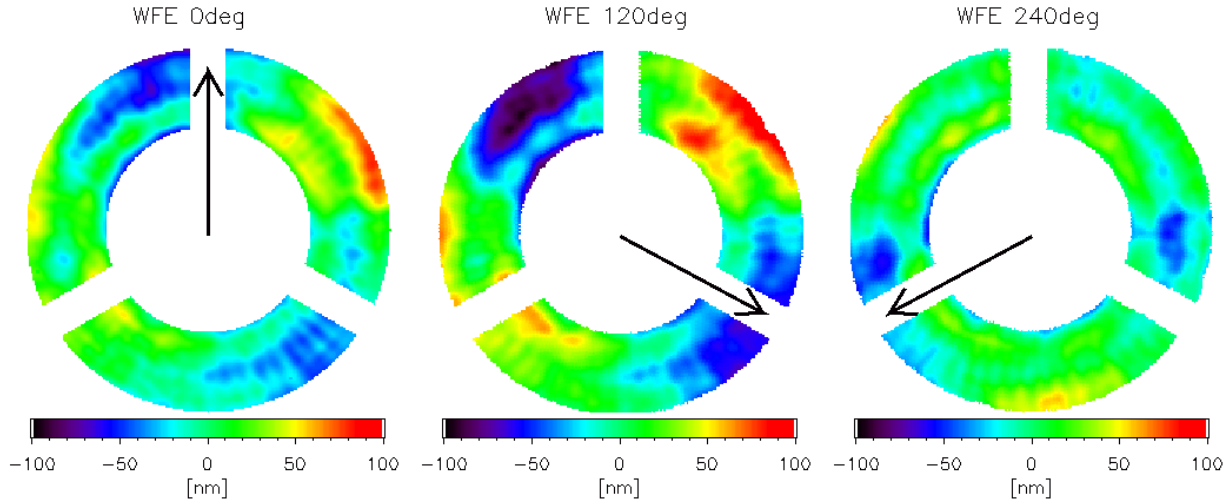

Figure 10. WFE map measured after the final alignment of the secondary mirror, at 0° (lef), 120° (middle) and 240° (right) configurations. Black arrows show the direction of the gravity on each measurements. In 0° configuration image, downward direction correspond to +X direction and rightward direction correspond to +Y direction of the CLASP2 instrumental coordinate. Piston, tilt X/Y and defocus were removed.

Table 5. Aberrations from the 8th terms circular Zernike fitting on the WFE measurements and RMS WFE.

Configuration	Defocus	Astigma--tism 0°	Astigma--tism 45°	Coma Y	Coma X	RMS WFE
0°	-0.078λ	0.044λ	0.056λ	0.000λ	0.008λ	28.12 nm
120°	-0.075λ	0.015λ	0.120λ	-0.012λ	0.010λ	42.61 nm
240°	-0.101λ	-0.027λ	-0.017λ	0.007λ	-0.008λ	20.27 nm
Zero-G	-0.085λ	0.010λ	0.053λ	0.000λ	0.003λ	23.90 nm
Error (1σ)	$\pm0.017\lambda$	$\pm0.024\lambda$	$\pm0.023\lambda$	$\pm0.019\lambda$	$\pm0.016\lambda$	-

The Zero-G WFE (left panel of Figure 11) was calculated by averaging the WFEs measured at the three orientations of the telescope. The coma aberrations were successfully reduced to around 0.00λ which is much smaller than the measurement error ($1\sigma < 0.02\lambda$), by adjusting the secondary mirror tilt as explained in Section 5.1. Although the gravity effect is removed, as shown in the aberration coefficients of Zero-G WFE in Table 5, astigmatism (especially 45°) remains. However this is not a problem since the requirement for RMS spot radius was met as described below.

Spot shape in on-axis optical pass (right panel of Figure 11) is obtained using Zero-G WFE as shown in the left panel of Figure 11. The spot is obtained by the derivative in X direction and Y direction of the measured wave-front multiplying the focal length (2614 mm). To derive RMS spot radius, we calculate the root mean square of the distance from the optical axis of the i th ray (total number of rays is n) reaching at the position (x_i, y_i) as in the Equation (1). The resulting RMS spot radius at the center of the slit was estimated as 4.37 μm using Equation (1). This RMS spot radius was smaller than our requirement of 5.5 μm (Table 2). Furthermore, the RMS spot radius is smaller than that of CLASP telescope (i.e. 6.6 μm[13]). As discussed in Section 2.2.2, 8th terms circular Zernike fitting reduced the measurement error and allowed to reach the better optical performance (i.e. smaller RMS spot radius).

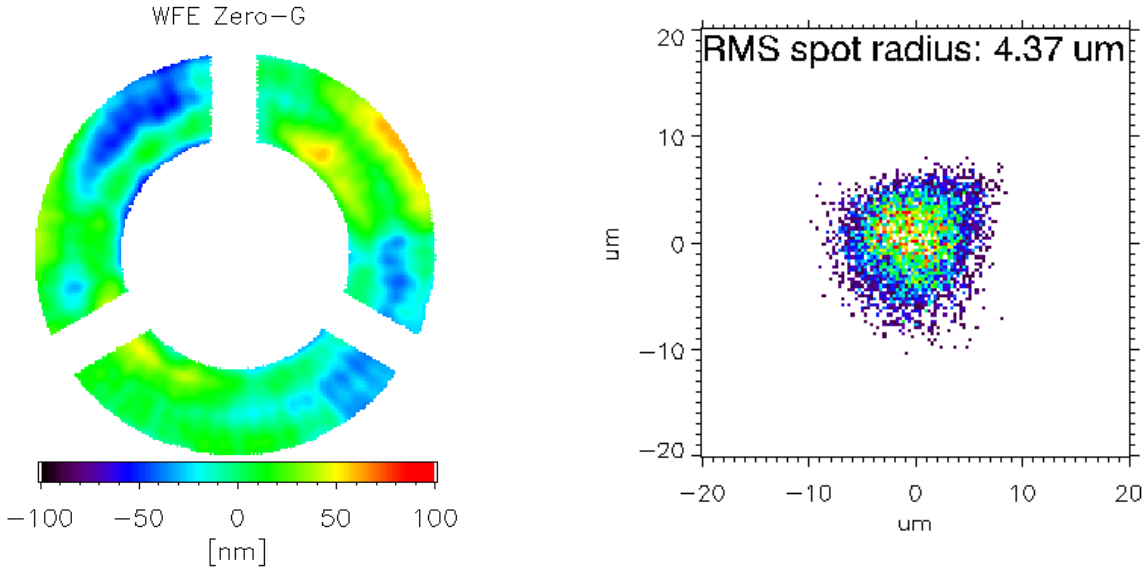

Figure 11. Left: Zero-G WFE (computed as the average of the three configurations) measured after the final alignment of the secondary mirror. Piston, tilt X/Y, defocus and gravity effect were removed. Right: Spot shape at the center of the FOV, estimated using the derivative of the Zero-G WFE.

$$r_d = \sqrt{\frac{1}{n}\sum_{i=0}^{n}(x_i^2 + y_i^2)} \tag{1}$$

5.3 Off-axis measurement

In this section, we present the results of WFE measurements on off-axis optical passes. As discussed in Section 1.1, the requirements for the RMS spot radius is determined at the edge of slit ($\pm 100''$ along X). However, taking into account SJ's FOV of $527'' \times 527''$ we performed the measurement at the FOV of (X,Y) = $(+200'', 0'')$, $(-200'', 0'')$, $(0'', +200'')$ and $(0'', -200'')$ by adjusting interferometer using the 6-axis stage, with respect to the slit (i.e. mirror target). The measurement results of off-axis optical pass are presented in Table 6. Coma Y increased by 0.054λ for X=$+200''$, and decreased by 0.018λ for X=$-200''$ compared with on-axis measurement. Similarly, coma X decreased by 0.006λ for Y=$+200''$ and increased by 0.029λ for Y=$-200''$. These trends are consistent with the simulation which predicts that the coma X(Y) emerges by $\pm 0.05\lambda$ at the FOV of Y(X) = $\pm 200''$. Table 6 clearly shows that the RMS spot radius was smaller than our requirement of 5.5 μm even in the field of view of $\pm 200''$. Therefore, the telescope alignment was succeeded to satisfy the requirement.

6. SUMMARY AND CONCLUSIONS

CLASP2 is a re-flight plan of the CLASP sounding rocket experiment and aims at the measurement of solar chromospheric magnetic fields via the Hanle and Zeeman effects in the Mg II h & k lines around 280 nm. After the recovery of the CLASP payload, we confirmed that the alignment of the telescope has not changed before and after the first flight by measuring the WFE with the He-Ne laser interferometer. After this confirmation, dual-band pass cold mirror coating targeting at the observation wavelengths of 121.6 nm and 280 nm was applied to the primary mirror. In the measurement after we installed the re-coated primary mirror, we found that misalignment occurred. Therefore, additional alignments were carried out and its performance meets the requirement. Although the primary mirror is almost transparent in visible light, we successfully performed the telescope alignment as in CLASP. In addition, we improved the analysis method, more precisely performed 8th terms circular Zernike fitting and reached the better performance than CLASP. Our analysis clearly demonstrated

Table 6. Aberration coefficients from the 8th terms circular Zernike polynomial fitting, RMS WFE without defocus, and corresponding RMS spot radius across the FOV.

X	Y	Coma Y	Coma X	RMS WFE	RMS spot radius
$0''$	$0''$	0.000λ	0.003λ	23.90 nm	4.25 μm
$+200''$	$0''$	0.054λ	0.014λ	26.53 nm	4.45 μm
$-200''$	$0''$	-0.018λ	-0.040λ	31.56 nm	4.83 μm
$0''$	$+200''$	-0.001λ	-0.003λ	29.94 nm	4.53 μm
$0''$	$-200''$	0.005λ	0.032λ	32.99 nm	4.57 μm

that the 8th terms circular Zernike polynomial fitting is effective to evaluate the optical performance of the telescope with relatively large central obscuration.

ACKNOWLEDGMENTS

The CLASP/CLASP2 team is an international partnership between NASA Marshall Space Flight Center, National Astronomical Observatory of Japan (NAOJ), Japan Aerospace Exploration Agency (JAXA), Instituto de Astrofísica de Canarias (IAC) and Institut d'Astrophysique Spatiale; additional partners are the Astronomical Institute ASCR, Istituto Ricerche Solari Locarno (IRSOL), Lockheed Martin and University of Oslo. The US participation is supported by the National Aeronautics and Space Administration under the CLASP2 grant issued through the Heliophysics Technology and Instrument Development for Science program. The Japanese participation is funded by the basic research program of ISAS/JAXA, JAXA small size project program, internal research funding of NAOJ, and JSPS KAKENHI (Grant Numbers 23340052, 24740134, 24340040, 25220703, and 16H03963). The French participation is funded by Centre National d'Etudes Spatiales (CNES). The Spanish participation is funded by the European Research Council (ERC) under the European Union's Horizon 2020 research and innovation programme (ERC Advanced Grant agreement No 742265).

REFERENCES

[1] Kano, R., Bando, T., Narukage, N., Ishikawa, R., Tsuneta, S., Katsukawa, Y., Kubo, M., Ishikawa, S., Hara, H., Shimizu, T., Suematsu, Y., Ichimoto, K., Sakao, T., Goto, M., Kato, Y., Imada, S., Kobayashi, K., Holloway, T., Winebarger, A., Cirtain, J., De Pontieu, B., Casini, R., Trujillo Bueno, J., Štěpán, J., Manso Sainz, R., Belluzzi, L., Asensio Ramos, A., Auchère, F., and Carlsson, M., "Chromospheric Lyman-Alpha Spectro-Polarimeter (CLASP)," in [*Space Telescopes and Instrumentation 2012: Ultraviolet to Gamma Ray*], *Proc. SPIE* **8443**, 84434F (2012).

[2] Kobayashi, K., Kano, R., Trujillo-Bueno, J., Asensio Ramos, A., Bando, T., Belluzzi, L., Carlsson, M., Casini, R., De Pontieu, B., Hara, H., Ichimoto, K., Ishikawa, R., Katsukawa, Y., Kubo, M., Manso Sainz, R., Narukage, N., Sakao, T., Štěpán, J., Suematsu, Y., Tsuneta, S., Watanabe, H., and Winebarger, A., "The Chromospheric Lyman-Alpha SpectroPolarimeter: CLASP," in [*Fifth Hinode Science Meeting*], Golub, L., De Moortel, I., and Shimizu, T., eds., *Astronomical Society of the Pacific Conference Series* **456**, 233 (2012).

[3] Narukage, N., Auchère, F., Ishikawa, R., Kano, R., Tsuneta, S., Winebarger, A., and Kobayashi, K., "Vacuum ultraviolet spectropolarimeter design for precise polarization measurements," *Appl. Opt.* **54**, 2080 (2015).

[4] Kano, R., Trujillo Bueno, J., Winebarger, A., Auchère, F., Narukage, N., Ishikawa, R., Kobayashi, K., Bando, T., Katsukawa, Y., Kubo, M., Ishikawa, S., Giono, G., Hara, H., Suematsu, Y., Shimizu, T., Sakao, T., Tsuneta, S., Ichimoto, K., Goto, M., Belluzzi, L., Štěpán, J., Asensio Ramos, A., Manso Sainz, R., Champey, P., Cirtain, J., De Pontieu, B., Casini, R., and Carlsson, M., "Discovery of Scattering Polarization in the Hydrogen Lyα Line of the Solar Disk Radiation," *ApJL* **839**, L10 (2017).

[5] Ishikawa, R., Trujillo Bueno, J., Uitenbroek, H., Kubo, M., Tsuneta, S., Goto, M., Kano, R., Narukage, N., Bando, T., Katsukawa, Y., Ishikawa, S., Giono, G., Suematsu, Y., Hara, H., Shimizu, T., Sakao, T., Winebarger, A., Kobayashi, K., Cirtain, J., Champey, P., Auchère, F., Štěpán, J., Belluzzi, L., Asensio Ramos, A., Manso Sainz, R., De Pontieu, B., Ichimoto, K., Carlsson, M., and Casini, R., "Indication of the Hanle Effect by Comparing the Scattering Polarization Observed by CLASP in the Lyα and Si III 120.65 nm Lines," *ApJ* **841**, 31 (2017).

[6] Belluzzi, L., and Trujillo Bueno, J., "The Polarization of the Solar Mg II h and k Lines," *ApJL* **750**, L11 (2012).

[7] Alsina Ballester, E., Belluzzi, L., and Trujillo Bueno, J., "The Magnetic Sensitivity of the Mg II k Line to the Joint Action of Hanle, Zeeman, and Magneto-optical Effects," *ApJL* **831**, L15 (2016).

[8] del Pino Alemán, T., Casini, R., and Manso Sainz, R., "Magnetic Diagnostics of the Solar Chromosphere with the Mg II h-k Lines," *ApJL* **830**, L24 (2016).

[9] Narukage, N., McKenzie, D., Ishikawa, R., Trujillo Bueno, J., De Pontieu, B., Kubo, M., Ishikawa, S., Kano, R., Suematsu, Y., Yoshida, M., Rachmeler, L., A., Kobayashi, K., Cirtain, J., Winebarger, A., Asensio Ramos, A., del Pino Alemán, T., Štěpán, J., Belluzzi, L., Larruquert, J., Auchère, F., Leenaarts, J., and Carlsson, M., "Chromospheric LAyer SpectroPolarimeter (CLASP2)," in [*Space Telescopes and Instrumentation 2016: Ultraviolet to Gamma Ray*], *Proc. SPIE* **9905**, 990508 (2016).

[10] Kubo, M., Katsukawa, Y., Suematsu, Y., Kano, R., Bando, T., Narukage, N., Ishikawa, R., Hara, H., Giono, G., Tsuneta, S., Ishikawa, S., Shimizu, T., Sakao, T., Winebarger, A., Kobayashi, K., Cirtain, J., Champey, P., Auchère, F., Trujillo Bueno, J., Asensio Ramos, A., Štěpán, J., Belluzzi, L., Manso Sainz, R., De Pontieu, B., Ichimoto, K., Carlsson, M., Casini, R., and Goto, M., "Discovery of Ubiquitous Fast-Propagating Intensity Disturbances by the Chromospheric Lyman Alpha Spectropolarimeter (CLASP)," *ApJ* **832**, 141 (2016).

[11] Ishikawa, S., Kubo, M., Katsukawa, Y., Kano, R., Narukage, N., Ishikawa, R., Bando, T., Winebarger, A., Kobayashi, K., Trujillo Bueno, J., and Auchère, F., "CLASP/SJ Observations of Rapid Time Variations in the Lyα Emission in a Solar Active Region," *ApJ* **846**, 127 (2017).

[12] Song, D., Ishikawa, R., Kano, R., Yoshida, M., Tsuzuki, T., Uraguchi, F., Shinoda, K., Hara, H., Okamoto, T., Auchère, F., McKenzie, D., Rachmeler, L., and Trujillo Bueno, J., "Optical Alignment of the High-Precision UV Spectro-Polarimeter (CLASP2)," in [*Space Telescopes and Instrumentation 2018: Ultraviolet to Gamma Ray*], *Proc. SPIE* **10699**, 10699-102 (2018).

[13] Giono, G., "Novel Instrumentation to Reach the 0.1% Polarization Accuracy for the Chromospheric Lyman-Alpha Spectro-Polarimeter," Doctoral dissertation of SOKENDAI (The Graduate University for Advanced Studies)(2016b).

[14] Giono, G., Ishikawa, R., Katsukawa, Y., Bando, T., Kano, R., Suematsu, Y., Narukage, N., Sakao, T., Kobayashi, K., and Auchère F., "Current progress of optical alignment procedure of CLASP's Lyman-alpha polarimetry instrument.," in [*Space Telescopes and Instrumentation 2014: Ultraviolet to Gamma Ray*], *Proc. SPIE* **9144**, 91443E (2014).

[15] Giono, G., Katsukawa, Y., Ishikawa, R., Narukage, N., Kano, R., Kubo, M., Ishikawa, S., Bando, T., Hara, H., Suematsu, Y., Winebarger, A., Kobayashi, K., Auchère F., and Trujillo Bueno, J., "Optical alignment of the Chromospheric Lyman-Alpha SpectroPolarimeter using sophisticated methods to minimize activities under vacuum.," in [*Space Telescopes and Instrumentation 2016: Ultraviolet to Gamma Ray*], *Proc. SPIE* **9905**, 99053D (2016a).

[16] Takeda, M., Ina, H., and Kobayashi, S., "Fourier-transform method of fringe-pattern analysis for computer-based topography and interferometry," *Optical Society of America* **72** (1) (1982).

[17] Narukage, N., Kubo, M., Ishikawa, R., Ishikawa, S., Katsukawa, Y., Kobiki, T., Giono, G., Kano, R., Bando, T., Tsuneta, S., Auchère, F., Kobayashi, K., Winebarger, A., McCandless, J., Chen, J., and Choi, J., "High-Reflectivity Coatings for a Vacuum Ultraviolet Spectropolarimeter," *Solar Phys.* **292**, 40 (2017).

[18] Ishikawa, R., Narukage, N., Kubo, M., Ishikawa, S., Kano, R., and Tsuneta, S., "Strategy for Realizing High-Precision VUV Spectro-Polarimeter," *Solar Phys.* **289**, 4727 (2014).